IL NUOVO CIMENTO **41 C** (2018) 110
DOI 10.1393/ncc/i2018-18110-0

COMMUNICATIONS: SIF Congress 2017

A monitored beam for precise neutrino flux determination: The ENUBET project

M. PARI([1])([2])

([1]) *INFN, Sezione di Padova - Via Marzolo 8, Padova, Italy*
([2]) *Università degli Studi di Padova - Via Marzolo 8, Padova, Italy*

received 30 January 2018

Summary. — In this paper we discuss the ENUBET experiment and explain how it can reduce by nearly one order of magnitude the flux-related systematics in accelerator neutrino beams. The ongoing research and development activities are described, together with the latest testbeam results from detector prototypes.

1. – Neutrino oscillations

Neutrino physics has seen a spectacular development in the last decades, culminating in the conclusive evidence for neutrino oscillations, the measurement of all mixing angles [1] and recent hints for leptonic CP violation [2]. Neutrino oscillations provide a firm evidence that neutrinos are massive particles, with non-degenerate mass eigenstates. Fermion mixing in the leptonic sector [3] is embedded in the weak charge current leptonic interaction Lagrangian as

$$\mathscr{L}^{CC}_{I,L} = \frac{g}{2\sqrt{2}}\,\bar{\nu}_{l_i}\,\gamma^{\mu}(1-\gamma^5)W_{\mu}\,U_{ij}\,l_j + \text{h.c.}, \tag{1}$$

where i and j are mass operator indexes and U is the PMNS mixing unitary matrix. The neutrino oscillation phenomenon originates from the massive nature of neutrinos and the presence of the mixing unitary matrix in eq. (1). The PMNS matrix links the neutrino mass eigenstates to a linear combination of them: the neutrino flavour states. The fact that we can only observe experimentally the neutrino flavour states and not their mass eigenstates leads finally to the oscillation phenomenon [4]. Hence, by exploiting the neutrino oscillations, much information about the Dirac part of the mixing matrix can be obtained, while it can be shown that nothing can be inferred about the Majorana phases from oscillations only.

Neutrino oscillation experiments are classified into several categories according to which oscillation effect they observe and to the neutrino source they employ. By defining

$P(\nu_\alpha \to \nu_\beta)$ as the oscillation probability from flavour α to β, an experiment aiming to measure $P(\nu_\alpha \to \nu_\alpha)$ is run in ν_α "disappearance" mode, while if it is aimed at measuring $P(\nu_\alpha \to \nu_\beta)$ with $\alpha \neq \beta$ it is run in ν_β "appearance" mode. Disappearance experiments are sensitive to mixing angles but cannot be used to establish three family interference effects that bring to CP violation.

The cross section for the neutrino interaction deeply changes at different neutrino energies, and in particular each class of experiments has developed specific experimental techniques with different systematic contributions.

Neutrinos for oscillation experiments are divided into solar, reactor, atmospheric and accelerator neutrinos. In this paper we will focus on accelerator neutrinos, which are generated by selecting secondary hadrons produced by a proton beam impinging on a target. The neutrinos are then produced by light mesons decays. In particular, the main contribution in a standard neutrino beam is given by charged pions, via the decay $\pi^\pm \to \mu^\pm + \nu_\mu/\bar{\nu}_\mu$. Kaons contribute usually to a smaller fraction of the produced beam, but, as we will see later, they will have an important role in the ENUBET experiment. The energy of accelerator neutrinos can be tuned by changing the primary proton energy and secondary hadrons momentum selection and it is typically in the 1–20 GeV range. The combined results of all the oscillation experiments lead to a unique determination of Δm^2_{21} and θ_{12}, with no dependence on the neutrino mass hierarchy. All the other 3ν parameters are correlated with the pattern of the neutrino masses either through matter effects (which depend on the sign of Δm^2_{32}) or through the interference of the oscillation terms, that depend on Δm^2_{31} and Δm^2_{32}. Hence, the determination of the mass hierarchy is of paramount importance to pin down the oscillation parameters and drive the experiments searching for neutrinoless double beta decay. In addition, the octant of θ_{23} is still not determined: there is a significant correlation between octant, mass hierarchy and the CP phase [5, 6]. CP violation in the leptonic sector has not been established yet and constraints on the CP phase are still rather loose. Accelerator neutrino experiments will thus have a key role in the solution to these open problems: for example, combining datasets from accelerator experiments in $P(\nu_\mu \to \nu_e)$ appearance mode at different baselines (*i.e.* the existing T2K and NOνA experiments) could tackle at the same time the CP-violation phase measurement and the mass hierarchy, exploiting the Earth matter effect [5]. Being these discoveries related to subleading effects with respect to what has been measured up to now, a higher precision is required by the future experiments. To give an example, the probability of the $\nu_\mu \to \nu_e$ oscillation is about 5%, *vs.* the 30% of $\nu_e \to \nu_e$ of solar experiments. Moreover the $\bar{\nu}_e$ cross section is substantially smaller than ν_e and a higher $\bar{\nu}_e$ flux is required to reach the same statistical precision. The situation is even worse in the direct comparison of the Δm^2_{31} and Δm^2_{32}, since the predicted value is of the same order as the present Δm^2 uncertainty. Finally, as it will be explained in the following section, limitations in the current neutrino beam experiments represent an important obstacle to reach higher precision.

2. – Current limitations in neutrino beams experiments

At present, the main limitation of accelerator neutrino beams resides in the limited knowledge of the neutrino flux at source. For this task a detailed hadronic beam and secondary production simulation, constrained by experimental hadron production data or near detector measurements, is usually employed, leading to an uncertainty of about 5–10% on the flux normalization. The world most accurate experiment is able to reach values as low as 7.8%, as described in [7]. This is still very far from the precision that

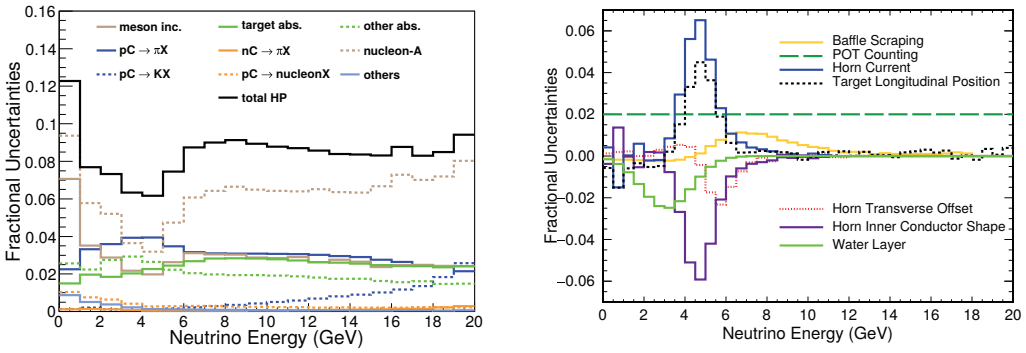

Fig. 1. – Main contributions to the uncertainty on the neutrino flux in the MINERνA experiment, from [7]. (a) Uncertainties on the NuMI low energy ν_μ "thin target flux" that originate from the hadron interactions along the beamline. (b) Beam geometry and focusing uncertainties on the ν_μ flux in the low energy beam configuration.

is needed for the next generation of long-baseline experiments. In fig. 1 there is an example of the typical uncertainty sources in a neutrino beam (MINERνA experiment in the present case). Figure 1a shows the hadron production related uncertainty, while fig. 1b shows the uncertainties related to the beamline geometry. The hadron production usually gives the dominant contribution. The classical solution for long-baseline experiments is to employ the near/far detector ratio in order to reduce the flux dependence. As an example, in the long-baseline MINOS experiment, flux systematics has been reduced to 3% [8]. Anyway this method does not apply for short-baseline experiments, and it is also troublesome for high precision appearance mode long-baseline experiments, since the final state has a different flavour and energy distribution due to oscillation. By considering, for example, the $P(\nu_\mu \to \nu_e)$ oscillation process, there are considerable theoretical uncertainties in the prediction of the σ_{ν_e} cross section [9]. A direct measurement of ν_μ and ν_e cross sections (both differential and total, depending on the downstream neutrino detector) at the per cent level strongly enhances the physics reach of long-baseline experiments reducing substantially the systematics on the near/far ratio. Unfortunately, no cross section is known with a precision better than 10%. The first reason for this is the above-mentioned 10% error on the initial neutrino flux. Additional systematics arise from nuclear effects in neutrino scattering, which highly depend on the neutrino energy scale. At the typical accelerator neutrino energies (from 1 to some tens of GeV) there are three main scattering mechanisms: quasi-elastic scattering, resonance production and deep inelastic scattering. In the first two processes the neutrino interacts with a single nucleon or bound nucleon pairs, while in the third process the neutrino resolves single quarks. The cross section of the three mechanisms depends in different ways on nuclear form factors, and in the deep inelastic case also on the parton distribution function. Accurate *ab initio* theoretical predictions are still missing.

It follows that a high precision experimental measurement of the neutrino cross section would be of great importance not only for oscillation experiments and the future objectives of neutrino physics, but also for shedding light on the theoretical model of the weak nuclear structure. This is even more relevant for the electron neutrino cross section, since $P(\nu_\mu \to \nu_e)$ and its CP conjugate are the main observables to determine the missing PMNS parameters. Still there are no high precision measurements of such a cross section. As explained before the error is dominated by the flux uncertainties and the current best measurements [10] are at the 20% level.

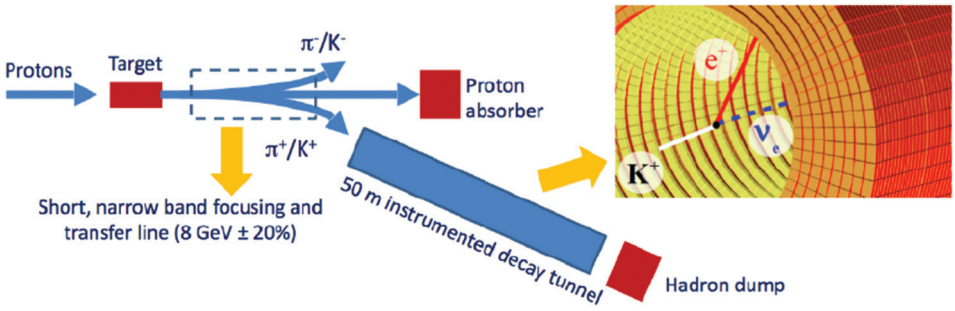

Fig. 2. – Schematic representation of the ENUBET beamline.

3. – The ENUBET experiment

The ENUBET (Enhanced NeUtrino BEam from kaon Tagging) project has been approved by the European Research Council (ERC Consolidation Grants 2015, Grant Agreement 681647) and aims at the solution of the previous problems. The goal is to design a facility to directly estimate the accelerator neutrino flux with an error of about 1% and use such a result to carry out a precise measurement of the electron neutrino cross section [11].

The basic idea is to instrument the decay tunnel with active material for particle detection. Figure 2 shows a schematic layout of the facility. After the proton beam is extracted from the ring and directed towards the target, the produced secondary hadrons are momentum and sign selected. Only π^+ and K^+ mesons arrive at the decay tunnel, where their decay will give rise to the neutrino beam. In a beamline configuration as the one depicted in fig. 2 the only relevant source of electron neutrinos is the semileptonic "K_{e3}" decay channel of K^+ particles:

$$K^+ \to \pi^0 e^+ \nu_e, \qquad \mathrm{BR}(K_{e3}) = (5.07 \pm 0.04)\%. \tag{2}$$

Being a three-body decay, the mean positron emission angle is 88 mrad, *i.e.* about 20 times larger than the mean muon emission angle of the leptonic dominant decays $\pi^+ \to \mu^+ \nu_\mu$ and $K^+ \to \mu^+ \nu_\mu$. Moreover, 88 mrad is also ~ 30 times larger than the beam divergence of undecayed particle. As a consequence, monitoring the large angle production of positrons instrumenting the walls of the cylindrical decay tunnel provides a direct means to evaluate the ν_e flux. In fact, neither the muons from the semileptonic decays of π^+ and K^+, nor the bulk of undecayed particles cross the calorimeter before reaching the beam dump. Hence the particle rate is much smaller than the rate in muon monitors of conventional neutrino beams [12], allowing for the exploitation of standard detector and readout technology. In such a way, a direct measurement of the positron flux on the instrumented tunnel translates in a measurement of the electron neutrino flux. By selecting secondaries with a large momentum, the ν_e component of the beam is mostly due to the K_{e3} decay of the kaons. Indeed, at a mean secondary momentum of 8.5 GeV/c the fluxes are

$$\frac{\Phi_{\nu_e}}{\Phi_{\nu_\mu}} = 1.8\% \ (\nu_e \text{ from } K_{e3}), \qquad \frac{\Phi_{\nu_e}}{\Phi_{\nu_\mu}} = 0.06\% \ (\nu_e \text{ from decay in flight of muons}) \tag{3}$$

and muon decay in flight contributions can be neglected.

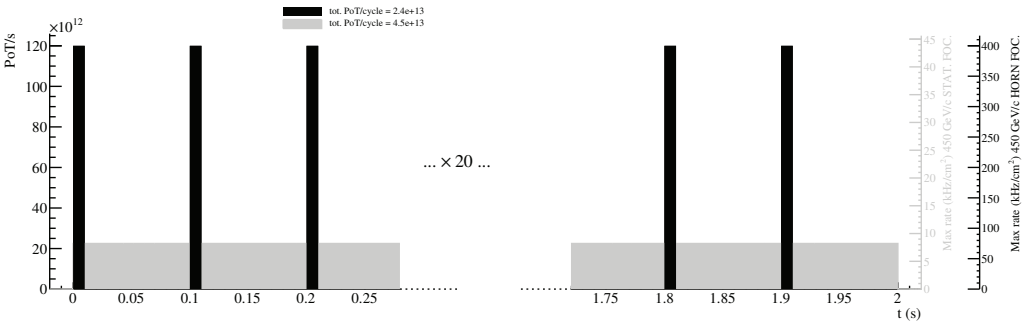

Fig. 3. – Proton extraction scheme during the 2 s flat top of the 15 s cycle of the CERN SPS in SRME mode (*i.e.* with twenty 10 ms long spills separated by 90 ms, in black) and slow resonant extraction mode (*i.e.* with a 2 s continuous long spill, in gray).

The calorimeter that we are designing to instrument the decay tunnel is described in [13]. Positron identification and e/π separation are performed using calorimetric techniques. The main detector is thus an iron-scintillator calorimeter with a transversal granularity of about 10 cm^2 and a longitudinal segmentation of about 4 radiation lengths. It must be noted however that pions are not a real background for the ν_e rate because they mostly originate from the other decay modes of kaons: ENUBET is also planning to study other decay modes to include this information. The constraint of having a low pile up probability fixes the local particle rate R at the detector surface to 0.5 $\mathrm{MHz/cm}^2$ through the relation

$$P = R\,S\,\Delta T_{cal}, \tag{4}$$

where S is the tile size (~ 10 cm^2), ΔT_{cal} is the recovery time (~ 10 ns) and P the pile up probability, that results of 0.05. This constraint generates important consequences on the proton extraction scheme of the beamline. Figure 3 shows, in black, the possible way in which the proton extraction method could be operated in order to be compatible with the maximum rate sustainable by the calorimeter. This operation mode is called slow resonant multiple extraction (SRME) mode and consists in a 10 ms spill of 1.2×10^{12} protons repeated every 100 ms. At the end of the 2 s flat top the SPS will be half-depleted. This operation mode allows for the use of magnetic horns [12] as focusing system, which would lead to a neutrino flux one order of magnitude higher with respect to a static focusing case. Such a 10 Hz (multiple) repetition of the actually tested slow resonance extraction mode (SRE, gray in fig. 3) is a scheme that has not been tested at the SPS up to now and it is one of the goals of ENUBET. In order to reach a statistical precision of 1% (*i.e.* $\simeq 10^4 \nu_e^{\mathrm{CC}}$) on a 500 t neutrino detector at 100 m from the beam dump, the required total number of protons on target is 5×10^{20} for a 30 GeV proton beam. This result corresponds to one year of data taking. The run time is reduced by increasing the proton beam energy. In the limit of 450 GeV protons the acquisition time will be less than two months. On the opposite side the development of a SMRE scheme is not an easy task and has the drawback that magnetic horns cannot be pulsed for a time period longer than about 10 ms (due to Joule eating). Hence, ENUBET will also consider the deployment of a static focusing system, in which there are no intrinsic limits for the focusing time (gray plot fig. 3) and that would lead to a reduced pile-up at the tagging calorimeter.

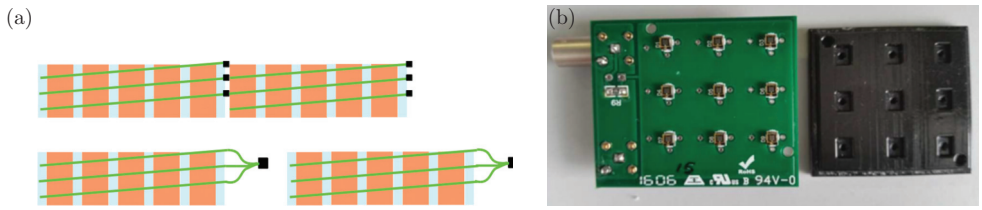

Fig. 4. – Details of the direct fiber-SiPM coupling implementation. (a) Fiber bundling (bottom) *vs.* direct coupling SiPM/fiber (top). The latter method allows for a compact longitudinal segmentation. (b) PCB for the direct SiPM coupling (left) and mechanical support (right) for optimal coupling.

The ENUBET proposal focuses on the construction of the instrumented decay tunnel facility, while an existent neutrino detector could be employed for the cross section measurement. The first goal is to prove the feasibility of the concept through a site-independent simulation of the beamline and a scaled prototype within 2021.

4. – Experimental apparatus and test

As explained in the previous section, the ENUBET experiment plans to instrument the decay tunnel of a conventional neutrino beam with a hollow-cylindrical calorimeter [11]. The granularity requirements ($\simeq$ 10 cm^2), fast response time ($\simeq$ ns) and the overall dimension ($\simeq$ 40 m) of the calorimeter limit the choice of the detector technology, cost-effectiveness being the main driver. The "shashlik" type calorimeter [14] fulfills the needs for a fast response time and cost effectiveness. It is a sampling calorimeter composed of scintillating active material interleaved with high density absorber tiles. The light signal is read out through wavelength shifter (WLS) optical fibers, in order to match the light pulse spectrum to the transfer function of the Silicon Photomultiplier (SiPM).

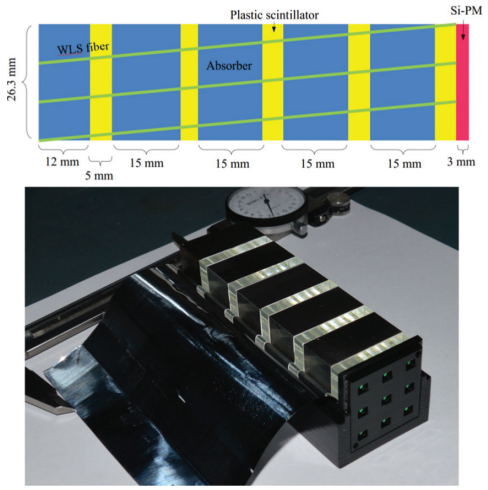

Fig. 5. – Shashlik calorimeter which will be the basic unit for the ENUBET tagger calorimeter. Scheme (top) and prototype (bottom).

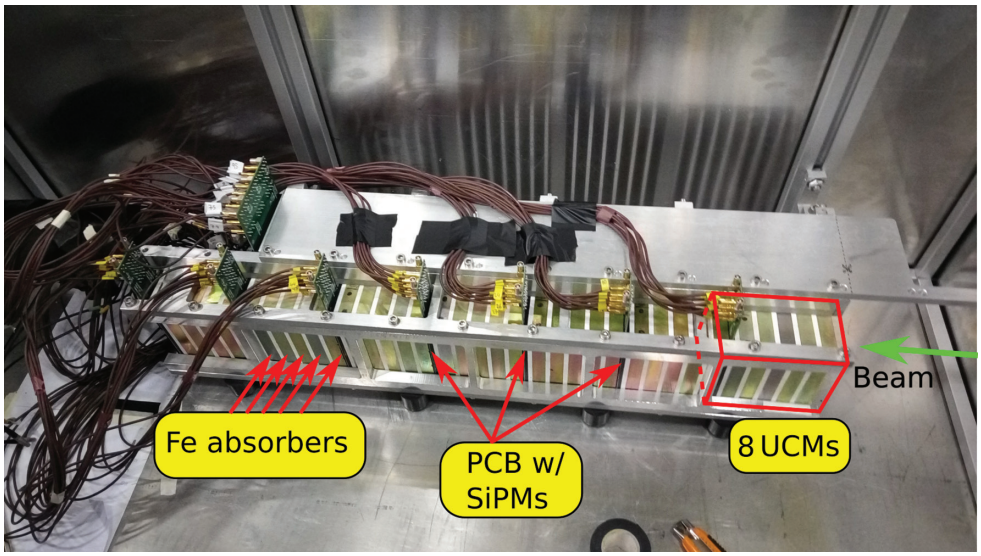

Fig. 6. – Calorimeter prototype tested at CERN PS-T9 beamline in November 2016.

The ENUBET and SCENTT collaborations have proven in [15, 16] that a light readout system where each WLS fiber is read by one single SiPM leads to a cheap and compact solution, with a performance equivalent to the standard PMT and fiber bundling readout methods. Figure 4a shows a schematic of direct fiber-SiPM coupling, while fig. 4b shows the readout PCB and mechanical support, both developed by the team.

Figure 5 shows the model and a prototype implementation of the ENUBET basic unit shashlik calorimeter, called Ultra Compact Module (UCM). 1.5 cm thick tiles of steel are interleaved with 0.5 cm tiles of plastic scintillator, and WLS optical fibers cross the entire length of the module. The fiber density is about one fiber per cm^2 and each of them is read by a single SiPM through the PCB of fig. 4b. A tagger calorimeter module made up of UCMs as described in [13] was prototyped and tested [17]. Figure 6 shows the calorimeter prototype tested on the November 2016 test beam at CERN PS-T9.

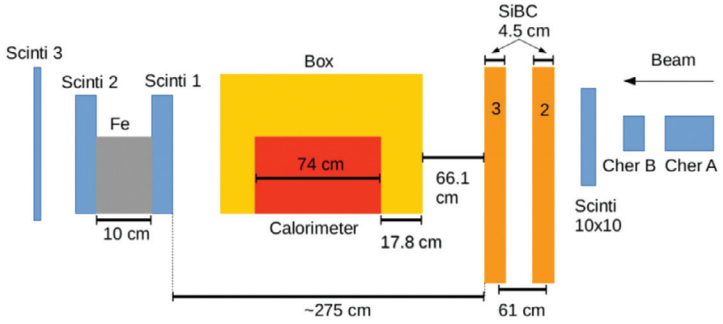

Fig. 7. – Layout of the instrumentation in the experimental area. Detectors include the calorimeter, two Cherenkov counters (Cher A and B), two silicon chambers (SiBC), the muon catcher (Scinti 1 and 2) and the trigger scintillator plane (Scinti).

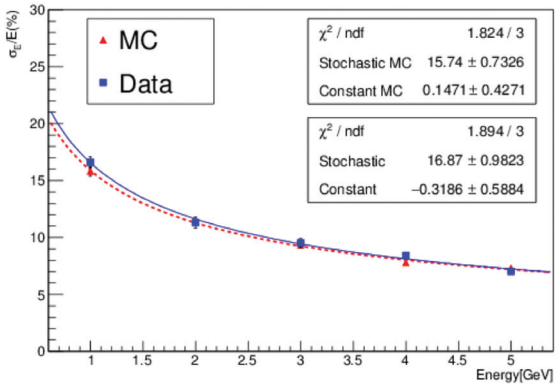

Fig. 8. – Energy resolution of the electromagnetic calorimeter at a tilt angle of 0 mrad.

The bottom part of the calorimeter (called "electromagnetic" and directly hit by the beam) is composed of 7 longitudinal blocks of 8 UCMs each. While the top part (called "hadronic") is a continuous 18-channel shashlik detector, employed to detect residual energy from hadronic showers.

Figure 7 provides a schematic view of the beamline. The particle beam is composed of electrons, muons and pions with energy up to 5 GeV. The particles are produced from the interaction of the primary proton beam (24 GeV/c) with a fixed target. Two CO_2 Cherenkov detectors (Cher A and Cher B) are used for particle identification. They are followed by a $10 \times 10\,\mathrm{cm}^2$ plastic scintillator (Scinti) that acts as a trigger for the data acquisition system. Two Silicon Chambers (SiBC) are used for the reconstruction of the particle track. They have a spatial resolution of about 30 μm. The calorimeter is inserted in a metal box in order to shield it from light and it is followed by a muon catcher composed of three scintillator slabs (Scinti 1, 2 and 3) and an iron absorber. An analysis

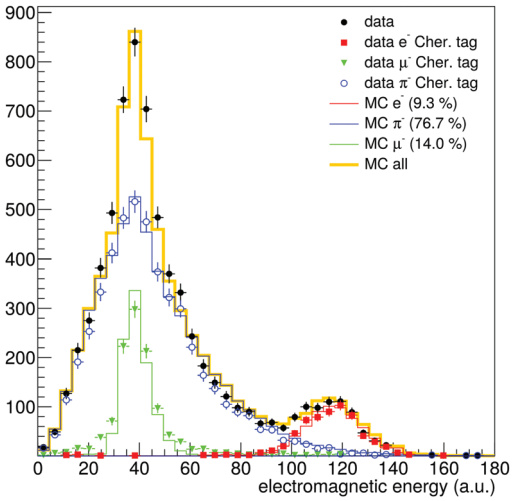

Fig. 9. – Distribution of the energy deposited in the scintillator (in MeV) for electrons, muons and pions in a 3 GeV, 0 mrad run.

of the electromagnetic calorimeter stochastic term has been carried out by measuring the electron energy deposited in the calorimeter. The electrons have been selected through the Cherenkov detectors and the events filtered by choosing a fiducial region around the center of the calorimeter, in order for an electromagnetic shower to be fully confined.

Figure 8 shows the energy resolution of the calorimeter (blue), compared to a Monte Carlo simulation (red), based on GEANT4 [18]. The points are fitted with a $\sigma_E/E(\%) = S/\sqrt{E\,(\mathrm{GeV})} \oplus C$ function, where S is the stochastic term and C the constant term and $\oplus$ indicates a quadratic sum. Compatible results were obtained at different tilt angles of the calorimeter with respect to the beam axis. This proves that the performance of the calorimeter is similar to the 0 mrad run in the angular range of interest for ENUBET. This behavior, which is very relevant for neutrino physics applications, is properly simulated by GEANT4.

Finally, the energy response of the detector (sum of the signal in all UCMs) for electrons, muons and pions at 3 GeV is shown in fig. 9, confirming a good agreement of the MC simulation with the experimental data.

5. – Conclusions

We have shown how ENUBET can lower the flux uncertainty in accelerator neutrino experiments by a factor of 10 by exploiting the K_{e3} decay channel: $K^+ \to \pi^0 e^+ \nu_e$. In the next 4 years ENUBET will investigate this technology and its application to a new generation of cross section experiments. During the first year of the project a rich simulation and prototyping program is giving very promising results. ENUBET is working to demonstrate that a "positron monitored" ν_e source can be built using existing technologies at CERN, FNAL or J-PARC giving a measurement of $\sigma(\nu_e)$ at 1% with a detector of moderate mass (~ 500 t).

* * *

This project has received funding from the European Unions Horizon 2020 Research and Innovation programme under Grant Agreement no. 654168 and no. 681647. The author gratefully acknowledges the ENUBET collaboration for support and inspiration, and the Italian Physical Society for the invitation to give the present review.

REFERENCES

[1] Particle Data Group (Patrignani C. *et al.*), *Chin. Phys. C*, **40** (2016) 100001.
[2] Wasko M., *T2K Status, Results, and Plans*, Talk at XXVIII International Conference on Neutrino Physics and Astrophysics, 4-9 June 2018, Heidelberg, Germany, DOI: 10.5281/zenodo.1286751, url: https://doi.org/10.5281/zenodo.1286751.
[3] Giunti C. and Kim C. W., *Fundamentals of Neutrino Physics and Astrophysics*, 1st ed. (Oxford University Press), 2007.
[4] Giunti C., *Theory of Neutrino Oscillations*, 2004, eprint: arXiv:hep-ph/0409230.
[5] Suekane F., *Neutrino Oscillations, A Practical Guide to Basics and Applications*, 1st ed. (Springer), 2014.
[6] Capozzi F., Lisi E., Marrone A., Montanino D. and Palazzo A., *Nucl. Phys. B*, **908** (2016) 218.
[7] MINERνA Collaboration, *Phys. Rev. D*, **94** (2016) 092005.
[8] Bishai M., *Nucl. Phys. B, Proc. Suppl.*, **229-232** (2012) 210.
[9] Day M. and McFarland K. S., *Phys. Rev. D*, **86** (2012) 053003.

[10] Bu X., *Measurement of Electron Neutrino Charged-Current Inclusive Cross Section in* 1−3 *GeV energy region with the NOνA Near Detector*, 2015, eprint: arXiv:hep-ex/1601.01213.
[11] Longhin A., Ludovici L. and Terranova F., *Eur. Phys. J. C*, **75** (2015) 155.
[12] Kopp S. E., *Phys. Rep.*, **439** (2007) 101.
[13] Longhin A., Ludovici L. and Terranova F., *Nucl. Instrum. Methods Phys. Res. A*, **824** (2016) 693.
[14] Fessler H., Freund P., Gebauer J., Glas K.M., Pretzl K.P., Seyboth P., Seyerlein J. and Thevenin J. C., *Nucl. Instrum. Methods Phys. Res. A*, **240** (1985) 284.
[15] Berra A. *et al.*, *IEEE Trans. Nucl. Sci.*, **58** (2011) 3.
[16] Berra A. *et al.*, *Nucl. Instrum. Methods Phys. Res. A*, **830** (2016) 345.
[17] ENUBET Collaboration (Ballerini G. *et al.*), *JINST*, **13** (2018) P01028.
[18] Agostinelli S. *et al.*, *Nucl. Instrum. Methods Phys. Res. A*, **506** (2003) 250.